CrossMark

29P/Schwassmann–Wachmann 1: A Rosetta Stone for Amorphous Water Ice and CO ↔ CO2 Conversion in Centaurs and Comets?

C. M. Lisse[1] , J. K. Steckloff[2,3] , D. Prialnik[4] , M. Womack[5,6] , O. Harrington Pinto[5] , G. Sarid[7] , Y. R. Fernandez[5,8] ,
C. A. Schambeau[5,8] , T. Kareta[9] , N. H. Samarasinha[2] , W. Harris[10] , K. Volk[10] , L. M. Woodney[11] , D. P. Cruikshank[5], and
S. A. Sandford[12]

[1] Planetary Exploration Group, Space Department, Johns Hopkins University Applied Physics Laboratory, 11100 Johns Hopkins Road, Laurel, MD 20723, USA
carey.lisse@jhuapl.edu
[2] Planetary Science Institute, 1700 E Fort Lowell Road, Suite 106, Tucson, AZ 85719, USA; jordan@psi.edu, nalin@psi.edu
[3] Department of Aerospace Engineering and Engineering Mechanics, University of Texas at Austin, Austin, TX 78712-1221, USA; steckloff@utexas.edu
[4] Department of Geosciences, Faculty of Exact Sciences, Tel Aviv University, Tel Aviv, Israel; dinak@tauex.tau.ac.il
[5] Department of Physics, University of Central Florida, Orlando, FL 32816, USA; mariawomack@gmail.com, oharrington@knights.ucf.edu, yan@ucf.edu,
dpcruikshank@comcast.net
[6] National Science Foundation, 2415 Eisenhower Avenue, Alexandria, VA 22314, USA
[7] SETI Institute, 339 Bernardo Avenue, Suite 200, Mountain View, CA 94043, USA; galahead@gmail.com
[8] Florida Space Institute, University of Central Florida, Orlando, FL 32816, USA; Charles.Schambeau@ucf.edu
[9] Lowell Observatory, 1400 West Mars Hill Road, Flagstaff, AZ 86001, USA; tkareta@lowell.edu
[10] Lunar & Planetary Laboratory, University of Arizona, Tucson, AZ 85721, USA; wharris@lpl.arizona.edu, kvolk@lpl.arizona.edu
[11] Department of Physics, Cal State University San Bernardino, 5500 University Parkway, San Bernardino, CA 92407, USA; woodney@csusb.edu
[12] Astrophysics Branch, Space Sciences Division, NASA/Ames Research Center, Moffett Field, CA 94035, USA; scott.sandford@nasa.gov

Abstract

Centaur 29P/Schwassmann–Wachmann 1 (SW1) is a highly active object orbiting in the transitional "Gateway" region between the Centaur and Jupiter-family comet (JFC) regions. SW1 is unique among the Centaurs in that it experiences quasi-regular major outbursts and produces CO emission continuously; however, the source of the CO is unclear. We argue that, due to its very large size ($\sim$32 km radius), SW1 is likely still responding, via amorphous water ice (AWI) conversion to crystalline water ice (CWI), to the "sudden" change in its external thermal environment produced by its Myrs-long dynamical migration from the Kuiper Belt to its current location at the inner edge of the Centaur region. It is this conversion process that is the source of the abundant CO and dust released from the object during its quiescent and outburst phases. If correct, these arguments have a number of important predictions testable via remote sensing and in situ spacecraft characterization, including the quick release on Myr timescales of CO from AWI conversion for any few kilometer-scale scattered disk Kuiper Belt Objects transiting into the inner system; that to date SW1 has only converted between 50% and 65% of its nuclear AWI to CWI; that volume changes on AWI conversion could have caused subsidence and cave-ins, but not significant mass wasting or crater loss; that SW1's coma should contain abundant amounts of CWI+CO_2 "dust" particles; and that when SW1 transits into the inner system within the next 10,000 yr, it will be a very different kind of JFC.

Unified Astronomy Thesaurus concepts: Centaur group (215); Comet surfaces (2161); Comet volatiles (2162); Comet interiors (272); Surface ices (2117); Comet nuclei (2160); Ice formation (2092)

1. Argument

Centaur 29P/Schwassmann–Wachmann 1 is a relatively large ($\sim$32 km radius; Schambeau et al. 2021a; Bockelée-Morvan et al. 2022[13]) icy planetesimal residing in a nearly circular orbit just beyond the orbit of Jupiter. It is well known for its unusually high level of CO production and dust emission

activity (but not conspicuously for any significant H_2O emission activity) and frequent outbursts (Senay & Jewitt 1994; Gunnarsson et al. 2008; Trigo-Rodríguez 2008, 2010; Hosek et al. 2013; Wierzchos & Womack 2020; etc.). Dynamically, Centaurs are an unstable transitional population, and they represent the middle state between the long-lived reservoir of icy Kuiper Belt Objects (KBOs) in the outer solar system and the quickly evolving short-period (SP) comet population in the inner solar system (see, e.g., reviews by Dones et al. 2015; Peixinho et al. 2020; Fraser et al. 2022). SW1 currently resides in a "Gateway" orbit: a collection of dynamical orbits that facilitate dynamical migration between these two populations (Sarid et al. 2019; Steckloff et al. 2020; Seligman et al. 2021). Sarid et al. (2019) showed that SW1's low-eccentricity orbit just exterior to Jupiter is typical for Centaurs transitioning to Jupiter-family comet (JFC) orbits and is very likely to undergo this transition within the next $\sim$10 kyr.

Starting in the 1970s, astronomical infrared spectral studies detected absorption features indicative of ices containing H_2O, CO, CO_2, CH_4, H_2CO, NH_3, and CH_3OH (Schwartz et al. 1973; Merrill et al. 1976; Soifer et al. 1979; Allamandola et al. 1992;

---

[13] For an assumed $p_v = 0.04$. There is a smaller published value of $R_{nuc} = 20 \pm 4$ km, $p_v = 0.13 \pm 0.04$ obtained by Cruikshank & Brown (1983) during a period of low SW1 nuclear activity. Reanalyzing the fluxes presented in the 1983 paper with modern thermophysical models, we find $R_{nuc} = 50 \pm 8$ km, $p_v = 0.02 \pm 0.01$. Thus, throughout this paper when we state $R_{nuc} = 32$ km, we are really saying $R_{nuc} = 32^{-14/+28}$ km. The net result is to broaden the estimated amorphous water ice (AWI) conversion timescales to 30–200 Myr (from 60 to 100 Myr), still very much comfortably $\gg$ the 10 Myr dynamical JSUN region crossing time (and a few Myr JS-region crossing time) for all currently plausible values of R_{nuc}.

Lacy et al. 1998) while investigating the composition of icy molecular cloud cores, the precursors to solar systems and their icy planetesimals. The spectral and physical properties of these ices, including their sublimation and condensation behaviors, were subsequently studied in the laboratory (see Lisse et al. 2021 and references therein) to investigate the possible makeup of these clouds and the plausibility that the laboratory ice analogs could be present in the molecular cloud at the ambient temperatures estimated from their spectroscopy. This work has been bolstered by spectral studies of ices detected on planetary satellites, Centaurs, Pluto, and KBOs in the outer solar system like H_2O, CH_4, N_2, CO, CO_2, CH_3OH, HCN, $NH_3 \cdot nH_2O$, and C_2H_6 (Cruikshank et al. 1998; Grundy et al. 2006; Brown et al. 2007; Barucci et al. 2008, 2011) and those detected in cometary comae as the products of sublimative mass loss from the parent nucleus, such as C_2H_2, C_3H_8, SO_2, and O_2 (Bieler et al. 2015; Mall et al. 2016). What is of most importance for this study of SW1 are the three most common species, H_2O, CO, and CO_2, which can be present as either pure or mixed ices, and in noncrystalline, amorphous, low-temperature kinetic product form (e.g., amorphous solid water ice = AWI; Stevenson et al. 1999; Kimmel et al. 2001; Dohnálek et al. 2003; Raut et al. 2007a, 2007b) or in higher-temperature, crystalline, lowest thermodynamic energy state form (e.g., crystalline water ice = CWI). For SW1, the properties and behavior of AWI and CWI are highly relevant, as there are a series of phase changes at low pressure in the 80–130 K temperature region from AWI to CWI, and T_{LTE}[14] for SW1 where it currently resides at 6 au is ∼115 K (after spending ∼4.5 Gyr in the Edgeworth Kuiper Belt (EKB) at $T_{LTE} = 30$–40 K). The crystallization transformation of *pure* AWI is moderately exothermic, but common volatile impurities in comets could render the process neutral to moderately endothermic (Kouchi & Sirono 2001). By contrast, CO ice sublimates fully in the 20–30 K range (Davidsson et al. 2021; Lisse et al. 2021, 2022; Steckloff et al. 2021, and CO_2 transforms from its amorphous to crystalline phase by ∼30 K (Escribanoa et al. 2013). We therefore expect SW1 to mainly consist of some sort of mixture of AWI, CWI, and crystalline CO_2 ices intermixed with rocky material and the minor ice species.

SW1 is special because it is very large compared to the typical "Gateway" Centaur/Comet. Sarid et al. (2019) estimate that only ∼4% of the objects reaching the Gateway are this size or larger. Its volume reserves of AWI ($\sim 4/3\pi \times$ [32 km]^3) are thus large enough versus the input solar energy flux (= $\pi \times$ [32 km]$^2 \times [1 - A_{bond}$[15]]) that $\tau_{thermal}$, the time it takes to convert all its AWI → CWI (the proposed activity driving process for Centaurs occurring inside 10 au; Prialnik et al. 1995; Jewitt 2009; Li et al. 2020), is 60–100 Myr (see Section 2.1). This is much longer than the ∼10 Myr it typically takes a KBO to travel from the outer solar system to 6 au (Volk & Malhotra 2008; Prialnik & Rosenberg 2009; Sarid et al. 2019; Di Sisto & Rossignoli 2020; Gkotsinas et al. 2022) and the few Myr the KBO resides inside 10 au (Saturn's orbit), meaning that it has not yet exhausted the supply of any AWI it

may have had while residing in the Kuiper Belt region, and it could *still* be undergoing AWI → CWI conversion today.

By contrast, any AWI in four other, much smaller Centaurs ($R_{nuc} = 1$–6 km) in similar Gateway orbits around the Sun (P/2010 TO20 LINEAR-Grauer, 423P/Lemmon, 2016 LN8, and 2019 LD2 (ATLAS); Sarid et al. 2019; Steckloff et al. 2020; Bolin et al. 2021; Kareta et al. 2021; Schambeau et al. 2021b) would have crystallized long ago, within 0.1–6 Myr of the start of their dynamical migration from the Kuiper Belt to the dynamical Gateway near Jupiter's orbit. Thus, these other objects, like all known kilometer-sized JFCs, should be depleted in AWI, and their current activity is likely dominated by the sublimation behavior of crystalline water ice and its entrained impurities.

In Sections 2–7, we outline the timescale calculations and supporting arguments for the AWI conversion hypothesis. In Section 8, we discuss how comparative remote sensing studies of the activity patterns of Centaurs and Gateway objects versus size, heliocentric distance, and dynamical age could shed light on whether or not their mass loss is driven by thermal wave interior propagation and AWI conversion. In Section 9, we examine the processes and morphologies created by AWI conversion that an in situ spacecraft mission could uniquely search for.

2. Supporting Arguments

2.1. Thermal Timescales

Central to our arguments is an understanding of the thermal history of heat flow through an icy, undifferentiated, yet geologically complex object like SW1. The expected dependence of the conversion timescale on body size can be understood in a number of ways: we start off with a very simple back of the envelope energy balance argument, then progress to a moderately simple argument invoking the results expected for heat flow in a uniform body of finite thermal diffusivity, and finally graduate to the much more sophisticated modeling of Prialnik et al. (2004, 2008) and Prialnik & Rosenberg (2009), which includes energy balance, finite heat flow, layering, and sublimative effects. We present all of these because the first two simplified approaches add value for the reader to understand the physics of the problem.

We first establish the thermal time constant for a response to a sudden (<∼10 Myr) change in the outside temperature/local insolation environment of SW1 using simple energy balance. Implicit in this argument is that the time-limiting step is the delivery of energy via insolation to the body, not the flow of heat from the surface to the interior of the body, and that energy inputs from short-lived radionuclides are negligible (Prialnik 2021; Steckloff et al. 2021). We argue via analogy using the modeling solutions found for a body similar to SW1 when it was in the Kuiper Belt: Arrokoth, a body about the same size as SW1, and the subject of the first-ever close flyby of a cold-classical KBO by a spacecraft on 2019 January 1. The New Horizons mission flew within 3500 km of the object and conducted many spectrophotometric imaging studies, finding a highly flattened, inactive object with about 1/2 the width and 1/3 the thickness of a sphere that has remained at ∼45 au from the Sun since its formation as a contact binary some 4.5 Gyr ago (Stern et al. 2019; McKinnon et al. 2020). Arrokoth has been the subject of several studies of its thermal behavior since (Davidsson 2021; Lisse et al. 2021, 2022; Prialnik 2021;

---

[14] $T_{LTE} = 282/\mathrm{sqrt}(r_h)$, the equilibrium temperature achieved by a uniformly illuminated blackbody at heliocentric distance r_h.

[15] $A_{bond} = L_{scattered}/(L_{scattered} + L_{emitted})$, where L = luminosity, or the sum total energy output, across all wavelengths and angles, of a body. A_{bond} varies from 0.01 at 0.5 μm to 0.2 at 10 μm (Schambeau et al. 2015, 2021a) but is always ≪1, and thus scattering of incident sunlight is relatively unimportant for SW1's overall energy balance.

Steckloff et al. 2021), in order to try to understand why there was no surrounding gas coma produced by sublimative activity of easily vaporized hypervolatiles like nearly pure phases of N_2, CH_4, or CO (Gladstone et al. 2022; Lisse et al. 2022). The results of these studies found that it took $\sim$20 Myr (range 1–40 Myr) once the protoplanetary disk (PPD) cleared and became optically thin to the Sun's radiaiton out to the Kuiper Belt for Arrokoth to lose all its hypervolatiles.

Knowing Arrokoth's thermal timescale for hypervolatile loss, we can scale it to determine SW1's thermal timescale for hypervolatile loss. In general, the timescale for which an ice inside a KBO, Centaur, or comet is transformed solely via radiative solar heating should go as[16]

$$\tau_{\text{thermal}} \sim [\text{Total Reservoir of ices to be transformed}$$
$$/\text{Rate of Energy Input for Transformation}]$$
$$\sim V_{\text{nuc}}/A_{\text{nuc}}$$
$$\times [\text{Surface Area for absorbing solar radiation}]$$
$$= 4/3\pi R_{\text{nuc}}^3/\pi R_{\text{nuc}}^2$$
$$\sim R_{\text{nuc}} [\text{for a spherical body}].$$

Using Arrokoth's measured dimensions from the New Horizons flyby (Stern et al. 2019) and Prialnik's (2021) $\sim$20 Myr timescale for loss of hypervolatiles, we can now produce a timescale estimate for SW1's loss of hypervolatiles. A spherical 32 km radius SW1-sized object should lose its hypervolatiles in the Kuiper Belt owing to the same sudden change in the local equilibrium temperature T_{LTE} (as the PPD cleared T_{LTE} increased from $\sim$20 to 40 K) in

$$\tau_{\text{thermal,SW1}} \sim \tau_{\text{thermal,Arrokoth}}$$
$$\times (V_{\text{nuc,SW1}}/V_{\text{nuc,Arrokoth}})/(A_{\text{nuc,SW1}}/A_{\text{nuc,Arrokoth}})$$
$$\sim 20 \text{ Myr} \times \frac{\left[\frac{4/3\pi(32 \text{ km})^3}{35 \text{ km} \times 17 \text{ km} \times 12 \text{ km}}\right]}{[\pi \times 32 \text{ km}^2/(35 \text{ km} \times 17 \text{ km} \times 0.5)]}$$
$$= 36 \text{ Myr},$$

where the factor of 0.5 has been introduced into the term for Arrokoth's surface area to allow for the fact that it is only face-on to the Sun for about 1/2 of its orbit. Thus, from exposed surface to volume energy balance considerations alone, SW1 should respond to a sudden large change in incoming insolation energy about twice as slowly as Arrokoth does, mostly as a result of SW1 being about 2 times larger in effective radius than Arrokoth. By contrast, this calculation suggests that a 1 km radius spherical "typical" comet nucleus will respond to a sudden insolation change by processing any easily vaporized ices within $\sim$1 Myr, while even a large Halley-sized $\sim$6 km radius body will do so within $\sim$6 Myr.

If instead we consider that thermal heat transport into and out of SW1 is the rate limiting step controlling AWI-to-CWI conversion, we find that the timescale required to convert SW1's will trend as R_{nuc}^2. This is because the heat depth penetration distance (l_{heat}) solution for the 1D radial heat flow equation assuming a step function heat input is given by

$$l_{\text{heat}} = \sqrt{\mathcal{H} t_{\text{warm}}}$$
$$l_{\text{heat}}^2 = \mathcal{H} t_{\text{warm}},$$

where $\mathcal{H}$ is the thermal diffusivity of the material (typically $\sim 1 \times 10^{-7}$ $m^2\,s^{-1}$ for cometary materials; Prialnik et al. 2004; Steckloff et al. 2021) and t_{warm} is the elapsed time. For this case, we consider the time SW1 has spent close enough to the Sun for the surface to be warm enough for AWI to crystallize (t_{warm}) and compare to the radius of the nucleus, R_{nuc}; so long as the heat penetration depth is less than the radius of the object, then it is possible for AWI to survive in the object's interior. Thus, AWI can survive so long as

$$\frac{R_{\text{nuc}}^2}{\mathcal{H}} > t_{\text{warm}}.$$

From direct calculation using $\mathcal{H} = 1 \times 10^{-7}$ $m^2\,s^{-1}$, AWI should be able to survive on the order of 290 Myr in the interior of SW1 while resident in the Gateway. Alternatively, Prialnik (2021) found that the crystallization timescale for Arrokoth, with $R_{\text{nuc\_eff}} = (35 \times 17 \times 12)^{1/3} = 19$ km, is $\sim$22 Myr; scaling this result to the $\sim$32 km radius size of SW1, for a t_{warm} that scales as radius squared, one finds a timescale of $\sim$62 Myr. Both of these estimates are in stark contrast to the timescales for more typical comet nuclei; using R_{nuc}^2 scaling, an $\sim$1 km radius nucleus would crystallize all its AWI on timescales of $\sim$0.06 Myr and an $\sim$6 km radius Halley-sized nucleus would exhaust its AWI after $\sim$2 Myr of continuously residing at $\sim$6 au.

Finally, we present the sophisticated modeling treatment of Prialnik (2021), which follows the changing internal structure of an icy SW1 nucleus reacting to solar heating, starting with a composition of CO-laden amorphous ice and rock, until the ice crystallizes throughout the body. The code solves coupled differential equations for energy and mass flows simultaneously, while allowing for internal heat sources like the heat of phase change and bodies consisting of many different ice species, each with their own effective heat of sublimation and crystallization. Energy can diffuse into the interior via solid-state conduction, radiation, and/or gas advection. We do not go into the details of the calculations more here, but we refer the reader to the most recent reviews of the models found in Prialnik et al. (2004, 2008) and Prialnik & Rosenberg (2009).

In applying the sophisticated Prialnik 1D code with the parameters listed in Table 1 to the case of SW1, we considered models of different radii, adopting SW1's orbit and an albedo of 0.062, and obtained upper limits for the time required for full crystallization by assuming that no heat is released by the crystallization process. Somewhat shorter timescales were obtained by assuming AWI crystallization to release heat in the amount of -45 $kJ\,kg^{-1}$. The results of this numerical model, assuming a chondritic abundance SW1 containing a 1:1 mixture of ice to rock with mean density $= 0.5$ $g\,cm^{-3}$, corresponding to a porosity of 0.65, are shown in Figures 1 and 2 and Table 2. The rate of advance of the crystallization front for a 30 km radius object may be inferred from the left panel of Figure 1, which shows the residual AWI volume as a function of time. The right panel shows the time for total conversion of all AWI in a body of radius R_{nuc}.

The model time estimates for SW1 to lose all its AWI fall between 60 and 100 Myr (Figure 1(a)), while a "typical" 1 km radius sized Gateway Centaur would lose all its AWI in the first 0.2–0.3 Myr, and even a 6 km radius "Halley-sized" Gateway Centaur would convert all its AWI in 4–6 Myr (Figure 1(b)).

It is noteworthy that for the adopted composition, $CO/H_2O = 0.05$ by mass, *the estimated current production*

---

[16] But Arrokoth is a very nonspherical body (Stern et al. 2019; Keane et al. 2022), so we use its actual dimensions in our calculation here.
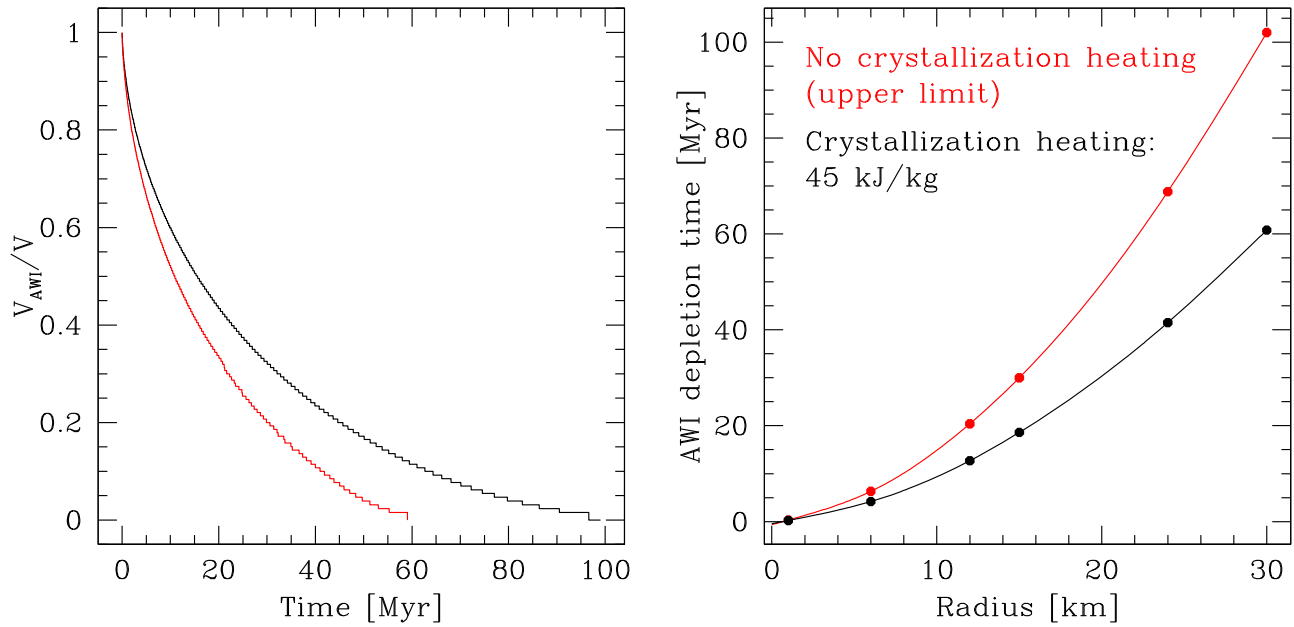
Figure 1. Prialnik model results for AWI depletion (via conversion to CWI) for SW1-like bodies of bulk chondritic abundance and 1:1 ice:rock ratio. In both plots the two curves are the results for assuming two different enthalpies for the AWI → CWI transition: red for $\Delta H_{\text{AWI conversion}} = 0$ kJ kg^{-1} energy released, which produces the slowest transformation rate, as there is no additional energy boost from the phase change itself to continue the process; black for $\Delta H_{\text{AWI conversion}} = -45$ kJ of heat released per kg of CWI produced. (Left) Fraction of AWI left after a given time for a spherical 32 km radius SW1-like body. Note that after 10 Myr, only ∼35% of the AWI in the $\Delta H = 0$ kJ kg^{-1} and 50% of the AWI in the $\Delta H = -45$ kJ kg^{-1} released case has transformed. (Right) Time for depletion of all AWI throughout the entire body. The $\Delta H = 0$ curve follows an approximate $R_{\text{nuc}}^{1.65}$ law and the $\Delta H = -45$ kJ kg^{-1} curve an approximate $R_{\text{nuc}}^{1.61}$ law.

Table 1
Prialnik Model Parameters

Parameter	Value
Ice heat capacity	7.5×10^4 T + 9.0×10^5 erg g^{-1} K^{-1}
Dust heat capacity	1.3×10^7 erg g^{-1} K^{-1}
Amorphous ice thermal conductivity	2.35×10^2 T + 2.82×10^3 erg cm^{-1} s^{-1} K^{-1}
Crystalline ice thermal conductivity	5.67×10^7/T erg cm^{-1} s^{-1} K^{-1}
Dust thermal conductivity	2×10^4 erg cm^{-1} s^{-1} K^{-1}
Crystallization rate	1.05×10^{13} $e^{-5370/T}$ s^{-1}
Latent heat of ice sublimation	2.8×10^{10} erg g^{-1}
Dust specific density	3.25 g cm^{-3}
Average pore size	0.1 cm

Note. The thermal conductivity is corrected for porosity (ψ) by a factor $(1 - \psi^{2/3})$ and includes radiative conductivity in pores.

rate of CO for SW1, ∼4 x 10^{28} mol s^{-1}, released from the AWI exceeds the sublimation rate of water ice at the surface by many orders of magnitude (Figure 2) and requires that the AWI conversion process be mildly exothermic, $\Delta H_{\text{AWI conversion}} \sim -45$ kJ kg^{-1} (or 1/2 the maximal $\Delta H_{\text{AWI conversion}} = 90$ kg kg^{-1} for pure water ice; Jewitt 2009). The estimated CO and H$_2$O gas production rates become comparable only when the AWI crystallization front has receded to ∼0.6 of the radius (after 30 Myr residence time at 6 au, $\Delta H_{\text{AWI conversion}} = -45$ kJ kg^{-1}; after 60 Myr residence time at 6 au, $\Delta H_{\text{AWI conversion}} = 0$).

We quote and use the results of the sophisticated modeling from this point forward. The important connection between the sophisticated model treatment and the two simple limiting cases given previously is that the curves of "sophisticated model" $\tau_{\text{AWI depletion}}$ versus R_{nuc}, trending approximately as $R_{\text{nuc}}^{1.63}$, fall between the small $\tau_{\text{AWI depletion}} \sim R_{\text{nuc}}^1$ behavior predicted for energy delivery limited behavior and the large $\tau_{\text{AWI depletion}} \sim R_{\text{nuc}}^2$ behavior predicted for heat flow limited behavior. On the other hand, neither of the simple estimates accounts for potential internal sources of heat, and these can have a very large effect on the time until total AWI depletion, as can be seen by comparing the two curves spanning the literature range of possible heats of AWI → CWI conversion in Figure 1.

2.2. Dynamical Timescales

We now consider the movement of SW1 in the near-modern-day solar system, where SW1 moved from its initial Kuiper Belt orbit to its present position in the Jupiter gateway region. The inward motion of a scattered disk KBO is initially started by self-stirring of the EKB, and not by planetary perturbations, but once started on a planet-crossing trajectory, a KBO can be scattered inward from one giant planet to the next on Myr timescales, with the largest amount of time spent farthest out by Neptune, where the orbital dynamical times are the slowest (Volk & Malhotra 2008; Bonsor & Wyatt 2012). While the exact dynamical path followed by an individual body depends sensitively on its initial state vector and the location of the planets (i.e., is highly chaotic), the median scattering time $\tau_{\text{dynamical}}$ is ∼10 Myr (with 90% of objects in the range 5–20 Myr; Volk & Malhotra 2008; Prialnik & Rosenberg 2009; Sarid et al. 2019; Di Sisto & Rossignoli 2020; Gkotsinas et al. 2022).

This dynamical inward motion would have caused a concomitant large increase in T_{LTE} for a KBO, increasing it from the 30–40 K typical of Kuiper Belt environments up to the
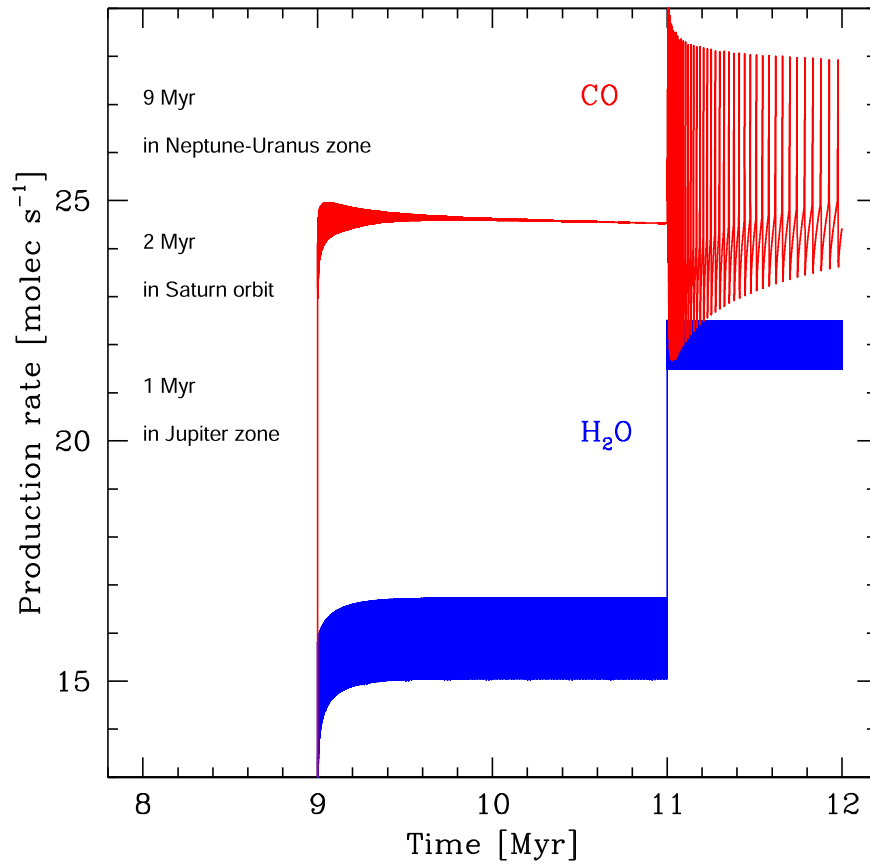
Figure 2. Relative CO and H_2O gas production rates for the Prialnik model of Figure 1, assuming a 32 km radius, 5% CO/H_2O, 1:1 Ice/Rock (by mass) body that has spent 4.56 Gyr in the Kuiper Belt, then 9 Myr in the Neptune−Uranus region, 2 Myr near Saturn, and finally the last 1 Myr near Jupiter at 6 au. Other dynamical trajectories are possible, for example, a body that has slowly but monotonically inspiraled from ∼40 to ∼6 au rather than moved stochastically, and they produce similar $Q_{CO}/Q_{H2O} > 10^3$ production ratios. Exploring the expected relative outgassing rates of all the various possible dynamical pathways is beyond the scope of this paper and will be the subject of a future study. Note that the predicted gas production rates oscillate in time, suggesting a thermophysical mechanism for producing SW1's observed outbursts.

Table 2
Prialnik Model: Time in Myr Required to Convert All AWI to CWI

Radius (km)	$\tau_{AWI \to CWI}$ (Myr) for $\Delta H_{AWI \to CWI} = 10^{-3}$ kJ kg^{-1} ∼0	$\tau_{AWI \to CWI}$ (Myr) for $\Delta H_{AWI \to CWI} = -45$ kJ kg^{-1}
1	0.33	0.24
6	6.3	4.2
12	20	13
15	30	19
24	69	42
30	100	61

110–120 K found in the Jupiter Gateway region. Because dynamical and orbital timescales are much slower in the outer solar system (Kepler's laws), it takes ∼70% of the dynamical migration time to move a typical object from the EKB at 30–60 au to ∼10 au and T_{LTE} ∼ 90 K (Saturn's orbit). The rest of the time is spent by the body in the 90–110 K Jupiter–Saturn region, so we can expect processes happening at $T < 90$ K to be well completed during the ∼10 Myr of dynamical migration, as well as any 90–110 K processes that take only a few Myr (like AWI conversion in kilometer-sized "typical cometary"

bodies, or the four small known "Gateway" objects; Table 1, Figure 1; Fernandez et al. 2018). By contrast, 10 Myr is very short compared to any of the estimates (and especially the sophisticated model estimate of 60–100 Myr) for SW1's AWI conversion time. In fact, in 10 Myr SW1 is predicted to have transformed only 35%–50% of its AWI by the sophisticated model (Figure 1(a)).

This implies that 29P/Schwassmann–Wachmann 1 is in a fundamentally different kind of internal state than a typical SP comet, i.e., it is large enough that the majority of its interior is not yet affected by its new thermal environment closer to the Sun. Whereas all potential AWIs in comet nuclei of a more typical ∼1 km size have likely fully crystallized prior to entering the Gateway or JFC populations, the sheer size of SW1 suggests that its migration into the Gateway would have provided insufficient time to fully crystallize all AWIs present. Instead, SW1 may possess an actively advancing thermal front (∼90 K according to the sophisticated Prialnik model), where the thermal environment of the inner solar system is slowly imprinting itself over the thermal environment of the Trans-Neptunian Population, and crystallizing AWI as it propagates. *This is more like the internal case of a long-period comet, albeit with a rather thick layer of CWI near its surface.* This means that when SW1 transits the Gateway into the inner system in the next ∼10 kyr (Sarid et al. 2019), not only will it be the largest and brightest JF cometary object seen in the modern era, but it could also be a highly unusual one.

3. Comparison to Observations

In the next four sections we discuss how the proposed AWI → CWI conversion model matches our current observational understanding of SW1. We start with a quick general summary of SW1's known behavior and then dive deeper into four different important individual issues.

The scenario of ongoing AWI crystallization driving SW1's activity is consistent with the finding by Wierzchos & Womack (2020) that the outbursts of dust and of CO from SW1 are not always correlated and that SW1 produces large amounts of gaseous CO into its coma but only negligible amounts of gaseous H_2O (Ootsubo et al. 2012; Bockelee-Morvan et al. 2014; Bockelée-Morvan et al. 2022; Womack et al. 2017). Unlike the situation for an active comet within ~2 au of the Sun (for which subsolar temperatures approach ~200 K), at SW1's distance the bulk water-ice matrix (+ dust + other ice impurities) that makes up the comet nucleus is not very labile at the local equilibrium temperatures of ~110 K (Jewitt 2009; Lisse et al. 2021, 2022). Thus, we expect neither large-scale bulk mass removal from a water-ice-dominated object nor appreciable nuclear H_2O gas emission (Figure 2). Instead, there should be removal of excess molecular "impurities" over and above the amount storable in a CWI hydrate lattice, ≲20% of the total H_2O ice volume (Schmitt et al. 1989; Jenniskens & Blake 1996), and a very low level of water gas production, both from the nucleus and from days- to months-old icy coma dust that has had a long time to heat up in sunlight and sublimate as it flies away from the nucleus.

4. Dust Release

For SW1, we can distinguish three different types of emission activity from the nucleus: Dust + Gas (primarily CO) emission; Gas-only emission; and Dust-only emission. Each of these types is plausible for SW1 activity driven by AWI conversion, and a mix of all three behaviors could be what is creating the rather jumbled temporal history of SW1 quasi-periodic outbursts and quiescent behavior epochs observed over the past few decades.

Structural changes of bulk water-ice structures due to minor species removal or AWI → CWI volume phase changes can cause geomorphological rearrangements on icy bodies (see the arguments made for Arrokoth's geomorphological structures by Moore et al. 2020; Spencer et al. 2021). Such cave-in, landslide, and slumping sinkhole creation events could launch a small fraction of bulk material as "dust" (=rocky material + refractory ices and organics; Belton et al. 2008, 2011; Steckloff et al. 2016; Steckloff & Samarasinha 2018) outbursts as material fails and rearranges; as long as the rearrangement events create debris moving at velocities greater than $v_{escapeSW1} \sim 5.5\,\mathrm{m\,s^{-1}}$, that material will escape the surface and be launched into the coma.[17] Similar small-scale, localized mass-wasting processes have been proposed as capable of causing comet outbursts and maintaining activity (Steckloff et al. 2016; Steckloff & Samarasinha 2018). As a result, SW1's frequent outbursts could thus be driven by frequent significant changes to its surface topography as trapped gas erupts and simultaneously blows off dusty surface material, a picture

consistent with the arguments by Ivanova et al. (2011) that the surface layers of SW1 must be disrupted in order to create the amount of observed CO gas outflow.

Another possible mechanism for dust emission is CO gas entrainment of fine dust regolith. Unlike the case for JFCs in the innermost solar system, where even the bulk matrix water-ice-dominated material is subliming and releasing all its internal materials, including captured refractory dust, SW1's bulk water-ice matrix is overall stable under the solid–solid phase AWI → CWI crystallization process. Any dust will stay captured—until the previously mentioned shrinkage-driven morphological rearrangements occur and shards and pieces of water ice + rock are liberated. As long as these rearrangements produce sufficiently fine (submicron- to micron-sized[18]) water ice + rock rubble, the copious amount of CO gas emission ($\sim4 \times 10^{28}$ mol s^{-1} quiescent level or $\sim1 \times 10^{29}$ mol s^{-1} during outburst) can entrain this rubble and launch it into SW1's coma, especially on the day side near the subsolar point where local temperatures are the highest (Fink et al. 2021). The two processes are coupled; liberation of fine dust and CO gas are both required for dust to be released by entrainment. If fine dust regolith production due to surface rearrangement is continual, then the dust production would appear to be governed by the production rate history of entraining gas (primarily CO), and CO + dust emission is observed. If instead the supply of loosely bound, fine regolith is produced stochastically and infrequently via episodic surface failures, then the rate of fine rubble production rather than the rate of CO production controls the observed dust outflow behavior, causing the two to appear decoupled. A sudden increase in nuclear CO production during an epoch where no fine dust regolith is available could produce CO-gas-only outburst events. Conversely, if a sudden surface rearrangement (landslide, faulting, sinkhole creation, etc.) creates significant new reservoirs of fine dust after a long no-regolith epoch, then an apparent dust-only outburst could result during a CO-quiescent phase.

5. Lack of Bulk CO Ice

A counterargument to an object powered by AWI conversion that can be made is that the CO emission seen from SW1 is due instead to direct sublimation of large amounts of subterranean pure or nearly pure CO ice. However, if CO-rich hypervolatile

---

[17] The detailed Keane et al. (2022) "The Geophysical Environment of Arrokoth" study shows that equatorial surface regions of a similarly sized object rotating with 16 hr period are gravo-rotationally unbound, so the required imparted velocity to cause dust escape could be less.

[18] SW1's CO gas production rate, Q CO, is ~4 x 10^{28} molecules s^{-1} quiescent, up to 1 x 10^{29} mol s^{-1} in outburst (Festou et al. 2001; Gunnarsson et al. 2008; Jewitt et al. 2008; Wierzchos & Womack 2020). 4 x 10^{28} molecules s^{-1} is equivalent to a mass flux rate of 1.4e-7 kg m^{-2} s^{-1} for a 32 km radius spherical body. Assuming ideal gas outflow at $v = 400$ m s^{-1} at $T_{LTE} = 115$ K, this implies a local pressure of 8.6 x 10^{-6} Pa above a 0.5 g cm^{-3} mean density body with surface gravitational acceleration = $4/3G\rho R_{nuc} = 1.4$ x 10^{-3} m s^{-2}. Quiescent lofting of micron-sized particles of radius a will occur when $F_{pressure} = \pi\ a^2 * 8.6$ x 10^{-6} Pa $> F_{grav} = 4/3\pi\ a^3\rho * 1.4$ x 10^{-3} m^2 s^{-1} or for $a < 3/4 * 8.6$e-6 Pa/(500 kg m$^{-3} * 1.4$ x 10^{-3} m^2 s^{-1}) = 9.2 z 10^{-6} m = 9.2 μm, and up to 2.2 x 10^{-5} m = 22 μm in outburst. For comparison, the typical JFC at 1 au is capable of lofting up to ~10^4 μm = 1 cm sized particles. We note also that simple, flat surface models of comet activity (in which gas drag must also overcome grain–grain surface cohesion) suggest that gas drag alone is incapable of lofting grains off the surface (e.g., Gundlach et al. 2015; Jewitt et al. 2019). Nevertheless, given that comets are known to actively emit dust, these models must not be complete; more modern models account for comet activity being tied to areas of steep topography (Vincent et al. 2016), and note that the grains may already be in motion owing to, e.g., mass-wasting events (Britt et al. 2004; Steckloff & Melosh 2016; Steckloff & Samarasinha 2018). In this case, the gas does not need to overcome surface cohesion, but merely needs to blow fine dust grains away.
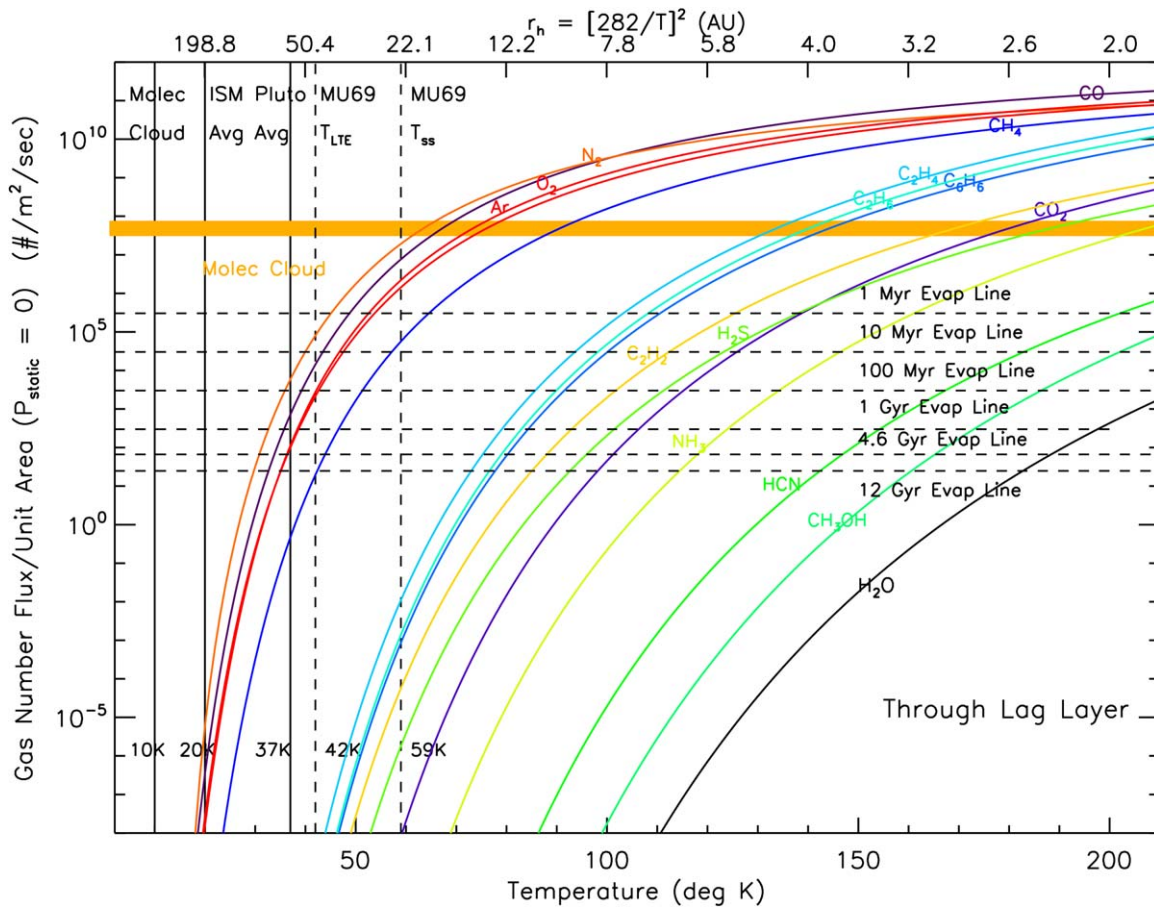
Figure 3. Species-specific Q_{gas} vs. temperature curves for species expected in comets, Centaurs, and KBOs. Horizontal dashed lines: values of the thermally driven outgassing rates at which an icy species is depleted in 1, 10, 100, 1000, 4600, and 12,000 Myr for an Arrokoth-sized body. Colored curves: loss rates for a piece of ice of labeled composition evaporating at temperature T after allowing for an overlying lag layer with thermal diffusivity $= 3 \times 10^{-7}$ s^2 m^{-1} impeding the flow of heat and gas into free space from the interior (Davidsson 2021; Prialnik 2021; Steckloff et al. 2021). Top axis: heliocentric distance from the Sun for a blackbody at local thermal equilibrium temperature T. From these curves and constraints, one can see that hypervolatile ices CO, N_2, and CH_4 are only stable in cold, dense molecular clouds and in modern KBOs residing beyond $\sim$100 au from the Sun, while metastable ices like CO_2 can survive in KBO and Centaur cores and hydrogen-bonded ices like H_2O can even survive on inner system comet surfaces. After Lisse et al. (2022).

ice were abundant, it would sublime vigorously at $\sim$20 K (less than its surface and interior temperature in the TNO population) and thus would have been lost during its billions of years of residency in the TNO population (Figure 3). Furthermore, the CO-rich ice should also be associated with N_2-rich phases, as N_2 gas is a species very similar in thermal sublimation properties to CO (Fray & Schmitt 2009; Lisse et al. 2021; Steckloff et al. 2021; Figure 3) that was roughly abundant at the 10% level versus CO in the gas phase of the protosolar nebula and in condensed phases of the PPD (Allamandola et al. 1992; Sandford & Allamandola 1993; Lacy et al. 1998; Kamata et al. 2019). Thus, N_2 should be present in large quantities in SW1's coma if sublimation of large amounts of pure CO ice had survived intact from SW1's initial formation and were driving the observed CO production, but it is tellingly only seen at the $\sim$0.01 level versus CO (as deduced from N_2^+ measurements; Korsun et al. 2008; Ivanova et al. 2016; Womack et al. 2017).

SW1 is thus very unlike hypervolatile-rich comet C/2016 R2 (likely a rare case of an object preserving its original PPD composition of majority hypervolatile ices in the Oort Cloud; Lisse et al. 2021, 2022) with $N_2/CO \sim 0.1$ (Wierzchos et al. 2017; Biver et al. 2018; McKay et al. 2019), consistent with the predicted value of $N_2/CO \sim 0.06$ for icy planetesimals forming

in the solar nebula at about 50 K (Owen & Bar-Nun 1995; Iro et al. 2003).

By contrast, AWI conversion would preferentially produce CO gas versus N_2 gas because CO's finite molecular dipole moment resulted in it becoming efficiently trapped in polar water-ice phases Gyr ago, forming a substantial CO molecule reservoir, while N_2's zero homonuclear diatomic dipole moment means that it was very poorly retained by polar water-ice phases making up the bulk of modern-day comets.

6. CO_2 Ice?

We have also considered bulk CO_2 ice as a possible source of the abundant CO gas emitted by 29P/SW1, but we reject it for two reasons. While evidence for bulk CO_2 ice was found in the gas and ice emitted by the dying core of comet 103P Hartley 2, verifying models of CO_2's survivability over 4.56 Gyr in the core of a small icy body (Davidsson 2021; Steckloff et al. 2021; Lisse et al. 2022), there is little to no evidence of CO_2 emission from SW1 (Ootsubo et al. 2012; Harrington Pinto et al. 2022). This is despite the fact that CO_2 sublimes rapidly into vacuum at $\sim$85 K, about the same temperature at which AWI ice recrystallizes (Fray & Schmitt 2009; Jewitt 2009; Lisse et al. 2021, 2022)—so we

would expect both AWI and CO_2 to be mobilized in SW1. Nor is impurity phase CO stable in bulk CO_2 ice above 30 K (i.e., the amorphous-to-crystalline transition for CO_2 ice occurs at 25–30 K; Escribanoa et al. 2013), making it only mildly more stable than the bulk CO removed within 1–40 Myr in KBOs (Davidsson 2021; Prialnik 2021; Steckloff et al. 2021). The finding that JFCs exhibit a strong correlation between their H_2O and CO_2 (but not CO) production rates seen by Harrington Pinto et al. (2022) is also highly consistent with CO_2 being housed in majority water-ice phases.

7. Lack of CO_2 Gas

The almost total lack of CO_2 outgassing activity from SW1 *is* nevertheless surprising and may be a significant observational constraint. As stated above, if AWI is active, then we would expect CO_2 ice also to be active (Steckloff et al. 2015; Steckloff & Jacobson 2016; Figure 3). Further, there is good evidence for CO_2 outgassing activity at the 2%–20% level versus water at $r < 2$ au in multiple comets (Colangeli et al. 1999; A'Hearn et al. 2011; Bockelée-Morvan & Biver 2017; Läuter et al. 2019; Harrington Pinto et al. 2022), suggesting that CO_2 should be abundant at the 2%–20% level versus H_2O in *all* KBOs, Centaurs, and comets.[19]

However, the lack of CO_2 in SW1 may simply be due to its observed high CO abundance level. CO abundances can vary quite widely in comets, ranging from <0.1 % up to ~15% versus H_2O (as measured for comets at $r_h < 2.5$ au when all three species are fully sublimating; Bockelée-Morvan & Biver 2017 and references therein; Harrington Pinto et al. 2022). A'Hearn et al. (2012), noting an apparent anticorrelation between the abundance of CO and CO_2 in comets (especially in CO_2-ice- and gas-rich comet 103P/Hartley 2, the second target of the Deep Impact mission; A'Hearn et al. 2011), argued from surveying a large number of comets that the quantity [CO + CO_2] in comets appears to be conserved, and by implication, the CO and CO_2 found in KBOs, Centaurs, and comets is sourced from the same reservoir. A recent survey of CO, CO_2 and H_2O gas production in 25 comets by Harrington Pinto et al. (2022) observed at $r_h < 2.5$ au has confirmed this, finding a median value of [CO + CO_2]/[H_2O] = 18% ± 4%. Whether this sourcing occurred in the protosolar nebula/giant molecular cloud phase or in the PPD phase is not yet clear; we do know that CO is highly abundant in the interstellar medium and, as the simpler molecule, was likely to have made up the majority of the original starting [CO+CO_2] reservoir (studies of dense molecular cloud core ices suggest [CO]/[CO_2] = 1 to 2; Suhasaria et al. 2017 and references therein).

On the other hand, the total amount of [CO+CO_2] versus water in SP comets, ~20% (Colangeli et al. 1999; A'Hearn et al. 2011; Bockelée-Morvan & Biver 2017; Läuter et al. 2019; Harrington Pinto et al. 2022), is interestingly about the same as the total carrying capacity of crystalline water ice's pore space for minority impurities. By contrast, the study of dense molecular cloud core ices suggests that PPD ices had [CO + CO_2]/[H_2O] = 45%–75% (Suhasaria et al. 2017 and references therein). As the laboratory work of Moore et al. (1991) and Pilling et al. (2010) has shown that it is very easy to interconvert between CO and CO_2 embedded in H_2O ice upon energetic charged particle radiation, this provides a plausible operative mechanism for producing large CO_2 abundances from initially high CO body abundances in icy bodies. If penetrating, ionizing radiation effects dominate, this could mean that the current CO_2 abundance in a comet is directly related to the ionizing radiation dose undergone by the original CO molecules in the original protosolar ices and thereafter in the aggregated icy body (Pilling et al. 2022). Thus, the relative CO_2/CO production ratio inside ~8 au, when both CO and CO_2 sublime vigorously (Lisse et al. 2021, 2022; Figure 3), could be a measure of the radiation exposure age of the CO_2-releasing ice, as well as the shielding effects of overlying layers.[20]

The preponderance of CO emission coupled with a lack of CO_2 activity suggests another possible mechanism controlling the AWI conversion. It is known from laboratory studies and observations of ISM ices that the CO in water ice resides on the surface of pores and that these pores coalesce as temperature increases, keeping roughly the same total volume while reducing their surface area for gas adsorption (Jenniskens & Blake 1996; Palumbo 2005; Bossa et al. 2014; Cazaux et al. 2015; David et al. 2019; He et al. 2019). This pore surface loss is the mechanism whereby internal AWI can slowly lose CO as it warms up from the 30–40 K temperatures of a Kuiper Belt to the ~90 K temperatures where AWI → CWI conversion occurs, and whereby large amounts of gas are evolved upon AWI → CWI crystallization. What is not commonly understood in the literature is the difference in the behavior of adsorbed CO versus CO_2 molecules in AWI as it begins to crystallize. He et al. (2016) have shown that in the temperature range of 88–105 K the sticking probability for CO to AWI is ~0, while that for CO_2 is in the range of 0.95–0.45. This will lead to preferential emission of CO and retention of CO_2 as AWI converts to CWI. What should thus be left behind as the thermal wave passes into the body are CO_2-rich water-ice phases, with CO_2 composing up to ~20% versus H_2O in the thermally mature CWI material (i.e., up to the impurity species carrying capacity of CWI; this is consistent with the finding by Harrington Pinto et al. 2022 for 25 comets with $r < 2.5$ au that CO_2 outgassing may be strongly tied to water production). How well this differential sticking probability segregates the CO versus CO_2 will depend on how slowly the thermal wave warming up the AWI and converting it into CWI propagates

---

[19] We note that 4.5 μm imaging data of SW1 obtained with Spitzer (Reach et al. 2013) and NEOWISE (Bauer et al. 2015) infrared space telescopes covered the combined emission bands of CO and CO_2 in this regime. Unfortunately, the CO and CO_2 emission could not be separated, and therefore no relative CO/CO_2 production rates could be obtained from these data. Although CO_2 production rates are cited in the tables of these papers, they are meant to be used as a proxy for the overall gas production rate and are not CO_2 production rates for SW1, a point explained in the original papers. The Q_{CO_2} values were derived assuming that all gaseous emission in the images was due to CO_2, not allowing for a mix of the two volatiles. As stated in those papers, SW1 is well known to have substantial CO production rates and Q_{CO_2} can be converted to Q_{CO} with a multiplicative factor of 11.6 (due to the difference in fluorescence efficiencies). Harrington Pinto et al. (2022) recently inferred CO_2 production rates from the Spitzer and NEOWISE imaging data using CO production rates from millimeter-wavelength spectra of CO obtained contemporaneously with the IRAM 30 m telescope. These inferred CO_2 production rates confirm that CO is produced in much higher quantity than CO_2 in SW1's coma.

[20] Note that we are only discussing CO and CO_2 trapped in AWI here; the observational evidence does not support CO emitted from SW1 via conversion of free CO_2 ice into free CO ice, unless this is happening as an ongoing process today that is transforming the CO_2 ice to CO ice with near 100% efficiency (a highly unlikely process; Pilling et al. 2022); otherwise, CO_2 gas would be detected in SW1's coma. This is because at the ~90 K temperatures required to convert AWI to CWI (Jewitt 2009), CO_2 ice is also very volatile (CO_2 flash sublimes into vacuum at 85 K, Escribanoa et al. 2013; the equilibrium saturation pressure is very large, Lisse et al. 2021; Figure 3).

into the body; as stated in Section 2, sophisticated models (Prialnik et al. 2004, 2008; Prialnik & Rosenberg 2009) have $\tau(R_{nuc}) \sim R^{1.63}$, $dR_{nuc}/dt \sim R^{-0.63}$, for both exothermic and non-exothermic AWI → CWI conversion (Figure 1), so larger bodies should segregate the two ices slower and more efficiently. Also consistently, the temperature of the phase front converting AWI to CWI in these numerical models is ~90 K, close to the optimal temperature for differential adsorption separation of CO from CO_2 in AWI.

Proving which of these plausible mechanisms (or combination thereof) are operant in small icy solar system bodies—a high initial CO/CO_2 abundance ratio coupled with a total fixed amount of $CO + CO_2$ in comets, radiation-driven conversion of $CO \leftrightarrow CO_2$ ice in AWI, or solid-state distillation via preferential sticking of CO_2 to AWI at 85–105 K—should be possible using detailed studies of an SW1 that is still actively transforming its AWI nearby. This is precisely why the title of this paper suggests SW1 as an excellent laboratory for studying AWI → CWI and $CO \leftrightarrow CO_2$ conversion, and in the next two sections we elaborate on potential future detailed studies of conversion-related processes that could be performed.

8. Remote Sensing Tests

From the arguments made above, we find that SW1's behavior makes a strong case for ongoing AWI crystallization, one that is often stochastic in its behavior, and in which the structure of SW1 is constantly being rearranged as a thermal wave warming the interior from ~40 to ~120 K propagates through a highly heterogenous and/or fractally connected body. This conversion should continue for Myr timescales as the Gateway thermal wave propagates deeper into the interior (somewhere on the order of (60–100 Myr thermal relaxation time)–(1 to 10 Myr dynamical emplacement time) = 50–100 Myr).

A number of remote telescopic investigations are immediately suggested by this line of reasoning. Further extension and testing of the Jewitt (2009) and Li et al. (2020) Centaur activity versus heliocentric distance findings is of course warranted, in order to further refine our understanding of the energy of activation and any $\Delta H_{AWI \to CWI}$ involved with SW1's activity. The total time for AWI conversion should scale roughly as the effective radius of the body to the 1.63 power (Prialnik et al. 2004, 2008; Prialnik & Merk 2008; Prialnik & Rosenberg 2009, Section 2.1), so population surveys of Centaur activity in large versus small Centaurs with $q < 10$ au (e.g., like those of Fernandez et al. 2018; Schambeau et al. 2021b) should be undertaken.

Also warranted are further searches for trends in CO versus CO_2 emission in Centaur and cometary bodies of known dynamical age. These would build on those carried out by Womack & Stern (1999), Wierzchos et al. (2017), and Harrington Pinto et al. (2022), but with emphasis on bodies of size between 6 and 30 km radius. If the CO-to-CO_2 conversion takes place inside the icy planetesimal (i.e., all icy solar system bodies started with reduced 100:0 ratios of $CO:CO_2$), then we can expect the largest bodies, like SW1, to shield their deep interiors and thus maintain their primordial CO molecules intact in their host H_2O ice matrix, while the smallest bodies that lack much mass shielding, like $R_{nuc} \sim 0.7$ km hyperactive comet 103P/Hartley 2 and $R_{nuc} \sim 2.4$ km comet 67P/C-G, should have converted most of their CO into CO_2. If instead preferential adsorptive sticking of CO_2 to AWI at 88–105 K is the dominant operative mechanism, we can

expect to find large amounts of CO_2- and water-ice-rich dust in large Centaur comae that is very slowly evaporating (this could explain the small but finite water gas emission and possible CO_2 gas emission seen for SW1 by Ootsubo et al. 2012; see Womack et al. 2017 and arguments therein; Bockelée-Morvan et al. 2022). To be specific, future ground- and space-based searches for water ice in SW1's coma and an extended coma icy dust source of water gas, ideally throughout epochs of both low and high emission activity, are warranted.

Parallel studies of Jupiter's Trojans as extremely old SW1 analogs are also warranted (e.g., Seligman et al. 2021), if they are indeed KBOs trapped into the L4 and L5 orbital resonances of the Sun–Jupiter system at $r \sim 5.2$ au at the time of the giant planet instability 3–5 Gyr ago. In this case, while coming from the same small-body feedstock, they would have Gyr ago converted all their AWI into CWI, and thus represent an AWI depleted end state. In this way they could be as much akin to the JFCs as we argue that still ~50% AWI-constituent SW1 is like an Oort Cloud comet (Section 2.2).

9. Future In Situ Spacecraft Measurements

Our AWI → CWI hypothesis also suggests tests to be done by in situ spacecraft directly investigating the chemistry and geomorphology of SW1. Previous experience with cometary in situ survey missions like Deep Impact and Rosetta has consistently turned up new regimes of behavior unobservable from Earth, for example, the sharp <10-minute rise times for comet 9P/Tempel 1's water sublimation rate upon nighttime water-ice frost rotating into sunlight (A'Hearn et al. 2005), or the neck striae and layering of 67P's lobes created by formation and evolutionary processes (Massironi et al. 2015; Ruzicka et al. 2019).

If we were observing the vigorous sublimation of *bulk* CO ice, we would expect it to occur with much surface mass removal and ejection of comingled dust, potentially producing the steep-walled pits seen on recent JFC 81P/Wild 2 (Brownlee et al. 2004) and KBO 2014 MU69 (Arrokoth; Singer et al. 2019a; Stern et al. 2019). The occasional extreme outburst could be due to pockets of CO gas buried beneath a lag layer requiring the buildup of significant overpressure before being released in a stochastic outburst accompanying blowout crater formation. Significant whole-body mass wasting would produce a relatively young surface geomorphology.

CO released from AWI instead should be comingled with other minor impurities present, and their release could be searched for by an in situ gas analyzer (although if sourced from depth, these minor impurities would have to be able to percolate out through $(T_{SubSolar} + T_{midnight})/2 \sim (150+30)/2 = 90$ K interior material; Huebner et al. 2006; Davidsson 2021; Lisse et al. 2021; Prialnik 2021; Steckloff et al. 2021). Impurity release caused by an AWI-to-CWI transition will not result in significant mass wasting, but subtler shrinkage effects due to the 2%–3% molar volume increase between low-density amorphous (LDA) water ice and crystal Ih water ice (Fraser et al. 2004; Palumbo 2005; Tanaka et al. 2019; this rises to an ~18% molar volume increase for transitions between high-density amorphous (HDA) water ice and crystalline Ih water ice), producing relatively gentle "subsidence" geomorphologies like depressions and folds (but not craters). The material left behind by AWI conversion coupled with CO gas evolution should be high strength and rich in CO_2 + crystalline water ice, with a preserved (although somewhat relaxed) cratering impact record.

AWI-conversion-driven outbursts could occur in the same fashion as for bulk CO ice, as the breakthrough of buried overpressured pockets, or by surface failure creating collapses that expose fresh ice-rich material, as seen in JFC 67P (Vincent et al. 2015, Steckloff et al. 2016; Pajola et al. 2017). The time required to build up enough pressure to create an overburden-failure caused outburst, coupled with predicted periodic thermophysical gas production excursions (Figure 2), could lead to quasi-periodic outgassing and outbursting behavior. This is in contrast to other outburst mechanisms such as those caused by landslides, which is a phenomenon primarily confined to the surface. Furthermore, the morphological manifestations of the outbursts caused by such different mechanisms would be different because of the associated geophysical differences. Therefore, nearly continuous high-resolution coma and surface morphology monitoring, ideally by an in situ rendezvous spacecraft mission (like the proposed AMBITION, Bockelée-Morvan et al. 2021; Centaurus, Singer et al. 2019b; or CHIMERA, Harris et al. 2019), over extended timescales (e.g., months to years), should yield critical clues to help resolve the drivers of activity in this enigmatic object.

Measurement of coma dust particles, by either direct sampling or spectroscopic mapping, can also provide telltale information. The low level of water gas production in SW1's coma, only seen in outburst (Bockelee-Morvan et al. 2010, 2014; Bockelée-Morvan et al. 2022), is likely due to the stability of crystalline water ice against sublimation at 6 au ($T_{LTE} \sim 115$ K, $T_{ss} \sim 161$ K; Ootsubo et al. 2012; Lisse et al. 2021, Figure 3). Therefore, coma grains surrounding SW1 should still contain much of their original water ice unless they are very old (i.e., far from the nucleus). Whether this water ice will be contained in separate ice particles containing refractory ices like H_2O, HCN, and CH_3OH (Lisse et al. 2021, 2022) or comingled as part of the "typical" dry cometary refractory ferromagnesian silicates and sulfides, future in situ sample collection and characterization measurements should find this "dust" to be very "wet" and water-ice rich. Finally, if the CO_2 preferential sticking mechanism of He et al. (2016) is important, this dust could also be CO_2-rich, at least in the inner coma regions where the dust has yet to warm up above ~ 105 K.

10. Conclusions and Recommendations

In this paper we have investigated the nature of 29P/Schwasmann–Wachmann 1, a large and unusual cometary Centaur. We have utilized thermophysical models including conversion of water ice from an amorphous to a crystalline state to show how 29P could still be, in the current day, harboring a large fraction of the AWI it started out with in the Kuiper Belt, and that AWI is currently undergoing crystallization within the deep interior, releasing highly volatile CO gas, and driving activity. We argue that this AWI $\rightarrow$ CWI conversion from the lower-density AWI to the higher-density crystalline water ice would be accompanied mainly by a compressional volume decrease, but not a large mass wasting, causing the nucleus to shrink, inducing interior and surface structural failures, which could be driving the frequently seen outbursts of this comet. Using the relative abundances for the majority species CO, CO_2, and H_2O seen in comets, we then show how 29P compares to other comets and fits into the evolutionary KBO $\rightarrow$ Centaur $\rightarrow$ SP comet evolutionary picture, concluding that 29P is evolving much slower than the
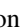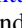
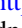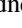"typical" kilometer-sized centaur and will become a very unusual JFC, full of AWI, when it transitions through the Jupiter dynamical gateway (Sarid et al. 2019).

If correct, our arguments have a number of important, testable predictions: the quick release on Myr timescales of CO from AWI conversion for any few kilometer-scale scattered disk KBOs transiting into the inner system; that to date SW1 has only converted between 50% and 65% of its nuclear AWI to CWI; that volume changes upon AWI conversion could have caused subsidence and cave-ins, but not significant mass wasting on SW1; that SW1's coma should contain abundant amounts of CWI CO_2-rich "dust" particles; and that when SW1 transits into the inner system within the next ~ 1 Myr, it will be a very different kind of JFC.

All of these findings are predicated on the assumption that AWI exists in KBOs and Centaurs and that AWI conversion, like direct water-ice sublimation, is a fundamental process that sculpts and alters icy bodies in the solar system. But unlike direct water-ice sublimation that drives inner solar system comet activity, it is poorly studied. As the closest known natural example of a body actively undergoing AWI conversion, we thus strongly recommend further intense study of 29P/SW1. This study should utilize both remote near-Earth based sensing characterization and monitoring (see Womack et al. 2020 and https://wirtanen.astro.umd.edu/29P/29P_obs.shtml), as well as direct exploration via a future in situ spacecraft mission (e.g., AMBITION, Bockelée-Morvan et al. 2021; Centaurus, Singer et al. 2019b; or CHIMERA, Harris et al. 2019).

ORCID iDs

C. M. Lisse https://orcid.org/0000-0002-9548-1526
J. K. Steckloff https://orcid.org/0000-0002-1717-2226
D. Prialnik https://orcid.org/0000-0002-6317-4839
M. Womack https://orcid.org/0000-0003-4659-8653
O. Harrington Pinto https://orcid.org/0000-0002-2014-8227
G. Sarid https://orcid.org/0000-0001-5678-5044
Y. R. Fernandez https://orcid.org/0000-0003-1156-9721
C. A. Schambeau https://orcid.org/0000-0003-1800-8521
N. H. Samarasinha https://orcid.org/0000-0001-8925-7010
W. Harris https://orcid.org/0000-0002-8378-4503
K. Volk https://orcid.org/0000-0001-8736-236X
L. M. Woodney https://orcid.org/0000-0002-0004-7381
S. A. Sandford https://orcid.org/0000-0002-6034-9816

References

A'Hearn, M. F., Belton, M. J. S., Delamere, W. A., et al. 2005, Sci, 310, 258
A'Hearn, M. F., Belton, M. J. S., Delamere, W. A., et al. 2011, Sci, 332, 1396
A'Hearn, M. F., Feaga, L. M., Keller, H. U., et al. 2012, ApJ, 758, 29
Allamandola, L. J., Sandford, S. A., Tielens, A. G. G. M., & Herbst, T. M. 1992, ApJ, 399, 134

Barucci, M. A., Alvarez-Candal, A., Merlin, F., et al. 2011, Icar, 214, 297
Barucci, M. A., Brown, M. E., Emery, J. P., & Merlin, F. 2008, in The Solar System Beyond Neptune, ed. M. A. Barucci et al. (Tucson, AZ: Univ. Arizona Press), 143
Bauer, J. M., Stevenson, R., Kramer, E., et al. 2015, ApJ, 814, 85
Belton, M. J. S., Feldman, P. D., A'Hearn, M. F., & Carcich, B. 2008, Icar, 198, 189
Belton, M. J. S., Thomas, P., Melosh, H. J., A'Hearn, M. F., & Veverka, J. 2011, EPSC-DPS Joint Meeting 2011, 1025
Bieler, A., Altwegg, K., Balsiger, H., et al. 2015, Natur, 526, 678
Biver, N., Bockelee-Morvan, D., Paubert, G., et al. 2018, A&A, 619, A127
Bockelée-Morvan, D., & Biver, N. 2017, RSPTA, 375, 20160252
Bockelee-Morvan, D., Biver, N., Crovisier, J., et al. 2010, AAS DPS Meeting, 42, 3.04
Bockelee-Morvan, D., Biver, N., Opitom, C., et al. 2014, in Asteroids, Comets, Meteors 2014, ed. K. Muinonen et al. (Helsinki)
Bockelée-Morvan, D., Biver, N., Schambeau, C. A., et al. 2022, A&A, 664, A95
Bockelée-Morvan, D., Filacchione, G., Altwegg, K., et al. 2021, ExA, in press (doi:10.1007/s10686-021-09770-4)
Bolin, B. T., Fernandez, Y. R., Lisse, C. M., et al. 2021, AJ, 161, 116
Bonsor, A., & Wyatt, M. C. 2012, MNRAS, 420, 2990
Bossa, J.-B., Isokoski, K., Paardekooper, D. M., et al. 2014, A&A, 561, A136
Britt, D. T., Boice, D. C., Buratti, B. J., et al. 2004, Icar, 167, 45
Brown, M. E., Barkume, K. M., Blake, G. A., et al. 2007, AJ, 133, 284
Brownlee, D. E., Horz, F., & Newburn, R. L. 2004, Sci, 304, 1764
Cazaux, S., Bossa, J.-B., Linnartz, H., & Tielens, A. G. G. M. 2015, A&A, 573, A16
Colangeli, L., Epifani, E., Brucato, J. R., et al. 1999, A&A, 343, L87
Cruikshank, D. P., & Brown, R. 1983, Icar, 56, 377
Cruikshank, D. P., Roush, T. L., Bartholomew, M. J., et al. 1998, Icar, 135, 389
David, R. O., Marcolli, C., Fahrni, J., et al. 2019, PNAS, 116, 8184
Davidsson, B. J. R. 2021, MNRAS, 505, 5654
Di Sisto, R. P., & Rossignoli, N. L. 2020, CeMDA, 132, 36
Dohnálek, Z., Kimmel, G. A., Ayotte, P., Smith, R. S., & Kay, B. D. 2003, JChPh, 118, 364
Dones, L., Brasser, R., Kaib, N., & Rickman, H. 2015, SSRv, 197, 191
Escribanoa, R. M., Muñoz-Caro, G. M., Cruz-Diazb, G. A., Rodríguez-Lazcanoa, Y., & Matéa, B. 2013, PNAS, 110, 12899
Fernandez, J. A., Helal, M., & Gallardo, T. 2018, PSS, 158, 6
Festou, M. C., Gunnarsson, M., Rickman, H., Winnberg, A., & Tancredi, G. 2001, Icar, 150, 140
Fink, U., Harris, W., Doose, L., et al. 2021, PSJ, 2, 154
Fraser, H. J., Collings, M. P., Dever, J. W., & McCoustra, M. R. S. 2004, MNRAS, 353, 59
Fraser, W. C., Dones, L., Nesvorny, D., Volk, K., & Womack, M. 2022, Comets III, in press
Fray, N., & Schmitt, B. 2009, P&SS, 57, 2053
Gkotsinas, A., Guilbert-Lepoutre, A., Raymond, S. N., & Nesvorny, D. 2022, ApJ, 928, 43
Gladstone, G. R., Lisse, C. M., Young, L. A., et al. 2022, PSJ, 3, 111
Grundy, W., Young, L., Spencer, J., et al. 2006, Icar, 184, 543
Gundlach, B., Blum, J., Keller, H. U., & Skorov, Y. V. 2015, A&A, 583, A12
Gunnarsson, M., Bockelee-Morvan, D., Biver, N., Crovisier, J., & Rickman, H. 2008, A&A, 484, 537
Harrington Pinto, O., Womack, M., Fernandez, Y., & Bauer, J. 2022, PSJ, 3, 247
Harris, W., Woodney, L., & Villanueva, G. 2019, EPSC, 13, 1094
He, J., Acharyya, K., & Vidali, G. 2016, ApJ, 823, 56
He, J., Clements, A. R., Emtiaz, S. M., et al. 2019, ApJ, 878, 94
Hosek, M. W., Blaauw, R. C., Cooke, W. J., & Suggs, R. M. 2013, AJ, 145, 122
Huebner, W. F. et al. (ed.) 2006, ISSI Scientific Report, Heat and Gas Diffusion in Comet Nuclei (Noordwijk: ESA)
Iro, N., Gautier, D., Hersant, F., Bockelée-Morvan, D., & Lunine, J. I. 2003, Icar, 161, 511
Ivanova, O. V., Luk`yanyk, I. V., Kiselev, N. N., et al. 2016, P&SS, 121, 10
Ivanova, O. V., Skorov, Y. V., Korsun, P. P., Afanasiev, V. L., & Blum, J. 2011, Icar, 211, 559
Jenniskens, P., & Blake, D. F. 1996, ApJ, 473, 1104
Jewitt, D. 2009, AJ, 137, 4296
Jewitt, D., Agarwal, J., Hui, M.-T., et al. 2019, AJ, 157, 65
Jewitt, D., Garland, C. A., & Aussel, H. 2008, AJ, 135, 400
Kamata, S., Nimmo, F., Sekine, Y., et al. 2019, NatGe, 12, 407
Kareta, T., Woodney, L. M., Schambeau, C., et al. 2021, PSJ, 2, 48
Keane, J. T., Porter, S. B., Beyer, R. A., et al. 2022, JGRE, 127, e07068

Kimmel, G. A., Stevenson, K. P., Dohnálek, Z., Smith, R. S., & Kay, B. D. 2001, JChPh, 114, 5284
Korsun, P. P., Ivanova, O. V., & Afanasiev, V. L. 2008, Icar, 198, 465
Kouchi, A., & Sirono, S. -i. 2001, GeoRL, 28, 827
Lacy, J. H., Faraji, H., Sandford, S. A., & Allamandola, L. J. 1998, ApJL, 501, L105
Läuter, M., Kramer, T., Rubin, M., & Altwegg, K. 2019, MNRAS, 483, 852
Li, J., Jewitt, D., Mutchler, M., et al. 2020, AJ, 159, 209
Lisse, C. M., Gladstone, G. R., Young, L. A., et al. 2022, PSJ, 3, 112
Lisse, C. M., Young, L. A., Cruikshank, D. P., et al. 2021, Icar, 356, 114072
Mall, U., Altwegg, K., Balsiger, H., et al. 2016, ApJ, 819, 126
Massironi, M., Simioni, E., Marzari, F., et al. 2015, Natur, 526, 402
McKay, A. J., DiSanti, M. A., Kelley, M. S. P., et al. 2019, AJ, 158, 128
McKinnon, W. B., Richardson, D. C., Marohnic, J. C., et al. 2020, Sci, 367, aay6620
Merrill, K. M., Russell, R. W., & Soifer, B. T. 1976, ApJ, 207, 763
Moore, J. M., Umurhan, O. M., White, O. L., et al. 2020, LPSC, 51, 1691
Moore, M. H., Khanna, R., & Donn, B. 1991, JGR, 96, 17541
Ootsubo, T., Kawakita, H., Hamada, S., et al. 2012, ApJ, 752, 15
Owen, T., & Bar-Nun, A. 1995, Icar, 116, 215
Pajola, M., Hofner, S., Vincent, J. B., et al. 2017, NatAs, 1, 0092
Palumbo, M. E. 2005, J. Phys.: Conf. Ser., 6, 211
Peixinho, N., Thirouin, A., Tegler, S. C., et al. 2020, in The Trans-Neptunian Solar System, ed. D. Prialnik, M. A. Barucci, & L. Young (Amsterdam: Elsevier), 307
Pilling, S., Carvalho, G. A., & Rocha, W. R. M. 2022, ApJ, 925, 147
Pilling, S., Seperuelo Duarte, E., Domaracka, A., et al. 2010, A&A, 523, A77
Prialnik, D. 2021, AAS/DPS meeting, 53, 307.10
Prialnik, D., Benkhoff, J., & Podolak, M. 2004, in Comets II, ed. M. C. Festou, H. U. Keller, & H. A. Weaver (Tucson, AZ: Univ. Arizona Press), 359
Prialnik, D., Brosch, N., & Ianovici, D. 1995, MNRAS, 276, 1148
Prialnik, D., & Merk, R. 2008, Icar, 197, 211
Prialnik, D., & Rosenberg, E. D. 2009, MNRAS: Lett., 399, L79
Prialnik, D., Sarid, G., Rosenberg, E. D., & Merk, R. 2008, SSRv, 138, 147
Raut, U., Famá, M., Teolis, B. D., & Baragiola, R. A. 2007a, JChPh, 127, 204713
Raut, U., Teolis, B. D., Loeffler, M. J., et al. 2007b, JChPh, 126, 244511
Reach, W. T., Kelley, M. S., & Vaubaillon, J. 2013, Icar, 221, 777
Ruzicka, B.-K., Penasa, L., Boehnhardt, H., et al. 2019, MNRAS, 482, 5007
Sandford, S. A., & Allamandola, L. J. 1993, ApJ, 417, 815
Sarid, G., Volk, K., Steckloff, J. K., et al. 2019, ApJL, 883, L25
Schambeau, C. A., Fernandez, Y. R., Lisse, C. M., Samarasinha, N., & Woodney, L. M. 2015, Icar, 260, 60
Schambeau, C. A., Fernández, Y. R., Micheli, M., et al. 2021b, CBET, 4992, 1
Schambeau, C. A., Fernández, Y. R., Samarasinha, N. H., et al. 2021a, PSJ, 2, 126
Schmitt, B., Espinasse, S., Grim, R. J. A., Greenberg, J. M., & Klinger, J. 1989, Physics and Mechanics of Cometary Materials, ESA SP-302 (Noordwijk: ESA), 65
Schwartz, P. R., Wilson, W. J., & Epstein, E. E. 1973, ApJ, 186, 529
Seligman, D. Z., Kratter, K. M., Levine, W. G., & Jedicke, R. 2021, PSJ, 2, 234
Senay, M. C., & Jewitt, D. 1994, Natur, 371, 229
Singer, K. N., Spencer, J.R., McKinnon, W. ., et al. 2019a, AGUFM, P33I-3535
Singer, K. N., Stern, S. A., Stern, D., et al. 2019b, in EPSC , 13, 2025
Soifer, B. T., Puetter, R. C., Russell, R. W., et al. 1979, ApJL, 232, L53
Spencer, J. R., Stern, S. A., Moore, J. M., et al. 2021, Sci, 367, aay3999
Steckloff, J., & Melosh, H. J. 2016, AAS/DPS Meeting, 48, 206.06
Steckloff, J. K., Graves, K., Hirabayashi, M., Melosh, H. J., & Richardson, J. E. 2016, Icar, 272, 60
Steckloff, J. K., & Jacobson, S. A. 2016, Icar, 264, 160
Steckloff, J. K., Johnson, B. C., Bowling, T., et al. 2015, Icar, 258, 430
Steckloff, J. K., Lisse, C. M., Safrit, T. K., et al. 2021, Icar, 356, 113998
Steckloff, J. K., & Samarasinha, N. H. 2018, Icar, 312, 172
Steckloff, J. K., Sarid, G., Volk, K., et al. 2020, ApJL, 904, L20
Stern, S. A., Weaver, H. A., Spencer, J. R., et al. 2019, Sci, 364, aaw9771
Stevenson, K. P., Kimmel, G. A., Dohnalek, Z., Smith, R. S., & Kay, B. D. 1999, Sci, 283, 1505
Suhasaria, T., Baratta, G. A., Ioppolo, S., Zacharias, H., & Palumbo, M. E. 2017, A&A, 608, A12
Tanaka, H., Yagasaki, T., & Matsumoto, M. 2019, JChPh, 151, 114501
Trigo-Rodríguez, J. M., García-Melendo, E., Davidsson, B. J. R., et al. 2008, A&A, 485, 599
Trigo-Rodríguez, Josep M., García-Hernández, D. A., Sánchez, Albert, et al. 2010, MNRAS, 409, 1682
Vincent, J.-B., Bodewits, D., Besse, S., et al. 2015, Natur, 523, 63

Vincent, J.-B., Oklay, N., Pajola, M., et al. 2016, A&A, 587, A14
Volk, K., & Malhotra, R. 2008, ApJ, 687, 714
Wierzchos, K., & Womack, M. 2020, AJ, 159, 136
Wierzchos, K., Womack, M., & Sarid, G. 2017, AJ, 153, 230

Womack, M., Sarid, G., Harris, W., Wierzchos, K., & Woodney, L. 2020, MPBu, 47, 350
Womack, M., Sarid, G., & Wierzchos, K. 2017, PASP, 129, 031001
Womack, M., & Stern, S. A. 1999, SoSyR, 33, 187